J Solid State Electrochem (2009) 13:445–453
DOI 10.1007/s10008-008-0582-7

ORIGINAL PAPER

Applications of nanostructured Pt-Au hybrid film for the simultaneous determination of catecholamines in the presence of ascorbic acid

Soundappan Thiagarajan · Shen-Ming Chen

Received: 26 March 2008 / Accepted: 1 May 2008 / Published online: 3 June 2008

Abstract Nanostructured platinum-gold (Pt–Au) hybrid film modified glassy carbon electrode (GCE) was fabricated by electro-deposition method in the presence of 2×10^{-4} mol l^{-1} L-cysteine. To examine the surface morphological analysis, the (Pt–Au) hybrid film were electrochemically deposited on transparent semiconductor indium tin oxide (ITO) electrodes for scanning electron microscopy (SEM) and energy dispersive spectroscopy (EDS) studies. From the SEM analysis, it was observed that the deposited nano-platinum (250–400 nm) was formed as a cauliflower-shaped structure with the gold nanoparticles (30–90 nm). The concentration variation of additive L-cysteine results in the formation of cauliflower-shaped platinum nanoparticles. Further, the Pt–Au hybrid film modified GCE could be used for the detection of catecholamine neurotransmitters epinephrine (EP), norepinephrine (NEP) individually and in the presence of ascorbic acid (AA) in pH 7 phosphate-buffered solutions (PBS). Furthermore, the proposed Pt–Au hybrid film could be applied for the detection of epinephrine in injection solution and ascorbic acid from commercially available vitamin C tablets.

Keywords Platinum nanoparticles · Gold nanoparticles · Epinephrine · Norepinephrine · Ascorbic acid

S. Thiagarajan · S.-M. Chen (✉)
Department of Chemical Engineering and Biotechnology,
National Taipei University of Technology,
No.1, Section 3, Chung-Hsiao East Road,
Taipei 106 Taiwan, Republic of China
e-mail: smchen78@ms15.hinet.net

Introduction

Catecholamine neurotransmitters were involved in all tissues, hormonal and neuronal systems for the regulation of physiological process. Therefore, it is important to develop a biosensor for the detection of epinephrine (EP), norepinephrine (NEP), neurotransmitters [1]. In particular, EP plays an important role in neurotransmitters and hormones, and is used in medicine for the treatment of heart attack, bronchial asthma, and cardiac surgery. Several analytical methods such as spectrophotometry [2], fluorimetry [3], liquid chromatography [4], capillary electrophoresis [5], chemiluminescence [6], electrochemiluminescence [7], amperometry [8], biamperometry [9], piezoelectric detection [10], and flow-injection procedures with electrochemical detection [11, 12] were reported for the determination of EP. However, some of these methods were expensive and the process complicated.

On the other hand, the NEP is one of the derivatives of catecholamine secreted in the adrenal medulla, which plays an important physiological role in the central nervous system. Its electrochemical detection was an important research for electroanalytical researchers and neurochemists [13]. Several available methods such as high-performance liquid chromatography (HPLC) [14, 15] and ion chromatography [16] have been reported for the determination of NEP. Next, the presence of ascorbic acid in both animal and plant kingdoms was found to be a vital component in human diet. Among the animal organs, the liver, leukocyte, and anterior pituitary lobe show the highest concentrations of AA. It is available in mammalian brain along with several neurotransmitter amines. Several methods like spectrophotometry [17], HPLC–UV [18], and liquid chromatography [19] have been reported for the determination of AA. Therefore, it is important to develop a simple and

rapid method for the determination of EP and NEP in the presence of ascorbic acid (AA).

Among many methods for the detection of EP and NEP, the voltammetric method has been found as a powerful tool for the detection of neurotransmitters. It is generally believed that the direct redox reactions of these species (EP, NEP with AA) at bare electrodes are irreversible, and over potentials are usually required for their amperometric detection. The direct redox reactions of these species at the bare electrodes take place at very similar potentials and often suffer from a pronounced fouling effect, which results in rather poor selectivity and reproducibility. For example, EP and AA always exist together in biological environment at most solid electrodes. AA largely coexists with EP, and their oxidation potentials largely overlap, so it is very difficult to determine the EP directly. It is well-known that EP exists as a cation and AA exists as an anion at physiological pH 7.0. In addition, AA oxidized at potentials close to that of the EP resulted in overlapping voltammetric response. For this reason, the chemically modified electrodes have been developed to eliminate the interference of AA to EP determination [8] and to separate the electrochemical response of EP and AA [20, 21].

Further, the oxidation potentials of AA overlaps with NEP, because AA largely co-exists with NEP in brain tissue, the content of which is 100–1,000 times higher than NEP. Thus, it is very difficult to detect NEP directly. To overcome this problem, the modified electrodes have been used to detect NEP. Next, in the modification of electrode surface, metal nanoparticles have led to some latest developments as a result of their characteristics, which are attributed to the ultra-small size, high surface area, and good biocompatibility. For example, the electrocatalytic activity of nanomaterials toward the electrochemical reactions of biomolecules such as EP [22], NEP [23], AA [24] has been extensively demonstrated. Especially, the platinum nanoparticles have evoked increasing interests in the design of sensors [25], and some reports have demonstrated that platinum nanoparticles can facilitate the electron transfer and increase the surface areas with enhanced mass transport characteristics. On the other hand, the voltammetric sensor based on gold nanoparticles for the determination of biological molecules such as NEP [26] has received more interest due to their good stability and biocompatibility. In addition, the seed-mediated growth of metal nanoparticles attached to indium tin oxide electrodes showed interesting results [27]. Furthermore, the L-cysteine, additive plays an important role in self-assembled monolayers. The size and crystalline structure of gold nanoparticles were controlled by using L-cysteine [28]. Not only were mono metallic nanoparticles reported to have additive L-cysteine, but also bi-metallic hybrid films [29]. In addition, carbon-supported bi-metallic Au–Pt nanoparticles for electrocatalytic methanol oxidation [30] and Au–Pt alloy nanoparticle catalysts for electrocatalytic oxygen reduction has been reported [31].

In this paper, we present a simple and direct procedure for the fabrication of nanostructured Pt–Au hybrid film based on the electrochemical deposition process. Further, the fabricated film was characterized by using scanning electron microscopy (SEM) and energy-dispersive X-ray spectroscopy (EDS Oxford 6587). The analytical applications of the film was ascertained by using the square wave voltammetry (SWV) and differential pulse voltammetry (DPV) techniques for the individual and simultaneous detection of neurotransmitters. In addition, the Pt–Au hybrid film has shown significant outcome for the simultaneous determination of EP and NEP in presence of AA. To examine the practical analytical utility of the proposed film, the simultaneous determination of EP in presence of AA from injection solution and tablets were examined and the results were found satisfactory.

Materials and methods

Reagents

Epinephrine, NEP, AA, and L-cysteine were purchased from Sigma-Aldrich (USA). $KAuCl_4{\cdot}3H_2O$ and K_2PtCl_6 were obtained from Strem Chemicals (Massachusetts, USA). The other reagents were of analytical grade. All the solutions were prepared with double distilled water. The whole experimental results were obtained at room temperature. The phosphate buffer pH 7 aqueous solutions (PBS) were prepared from 0.1 mol l^{-1} NaH_2PO_4 and 0.1 M NaH_2PO_4.

Apparatus

Electrochemical measurements like cyclic voltammetry (CV), square wave voltammetry (SWV) and differential pulse voltammetry (DPV) were carried out using CHI 900 potentiostats (CH Instruments, Austin, TX). A conventional three-electrode system was used throughout the experiments. The BAS glassy carbon electrodes (GCE) were in the form of disks (φ=0.3 cm in diameter) sealed in a Teflon jacket having an exposed geometric surface area of 0.07 cm^2. The working electrode was bare or nanostructured Pt–Au hybrid film modified GCE, the auxiliary electrode was platinum wire and Ag/AgCl electrode was used as a reference. All the potentials mentioned in this paper were referred to this reference electrode. The morphological characterization of the film was examined by SEM (Hitachi S-3000H). Here, for convenience,

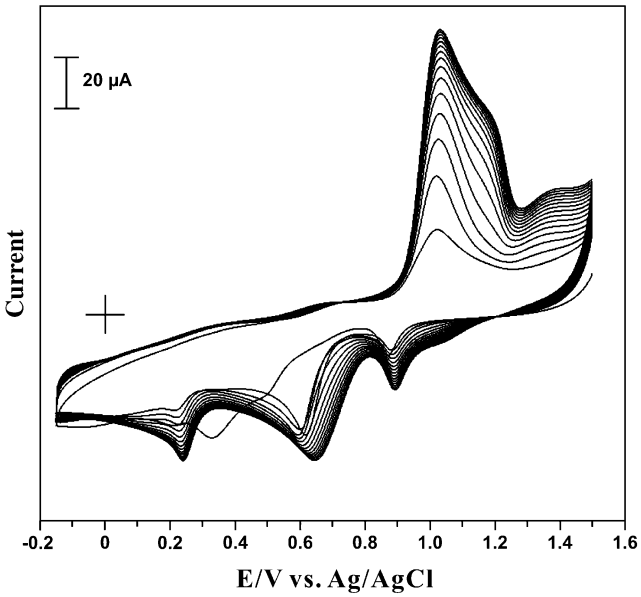

Fig. 1 Repeated cyclic voltammograms of nanostructured Pt–Au hybrid film deposited from 0.5 mol l^{-1} H_2SO_4 containing K_2PtCl_6 (4.9×10^{-4} mol l^{-1}), $KAuCl_4{\cdot}3H_2O$ (1.1×10^{-3} mol l^{-1}) in the presence of 2×10^{-4} mol l^{-1} L-cysteine for 30 cycles. Scan rate=100 mV s^{-1}

indium tin oxide (ITO) thin film coated electrodes were used for SEM imaging. Chemical analysis was carried out using energy-dispersive X-ray spectroscopy (EDS, Oxford, EDS-6587).

Preparation of nanostructured Pt–Au hybrid film

Before electro deposition of Pt–Au nanoparticles, the GCE was polished with the help of a BAS polishing kit with aqueous slurries of alumina powder (0.05 μm), rinsed and ultrasonicated in double-distilled deionized water. The Pt and Au nanoparticles were electrodeposited from acidic solution of 0.5 mol l^{-1} H_2SO_4 containing K_2PtCl_6 (4.9×10^{-4} mol l^{-1}), $KAuCl_4{\cdot}3H_2O$ (1.1×10^{-3} mol l^{-1}) in the presence of 2×10^{-4} mol l^{-1} L-cysteine for 30 cycles. Figure 1 shows the cyclic voltammograms of nanostructured Pt–Au hybrid film formation process. Here, the forward scan was initiated at 1.5 V and scanned toward the negative direction up to −0.15 V. It exhibited four peaks corresponding to reduction of Au at 0.89 V, L-cysteine (0.64 V), Pt (0.23 V) and for hydrogen adsorption at −0.11 V. In the reverse scan, the oxidations of Pt at 0.60 V, L-cysteine at 1.03 V, and Au at 1.19 V were obtained. On continuous cycling process, all the peaks were found growing. Here the redox peak of L-cysteine is obvious, and it was removed by careful washing with double-distilled water and in pH 7.0 PBS buffer solutions. From the growth of reduction and oxidation peaks of the Pt and Au, the depositions of the nanoparticles on GCE were ascertained.

Results and discussion

Electrochemical behavior of nanostructured Pt–Au hybrid film

The nanostructured Pt–Au hybrid film on GCE was transferred to de-aerated pH 7.0 PBS solution for the different scan rate studies as shown in Fig. 2. It shows that the film on GCE has two obvious cathodic peaks at −0.11 and 0.38 V for platinum and gold, respectively. The peak currents of platinum and gold were linearly increased with scan rates up to 500 mV s^{-1}. This result validates that the

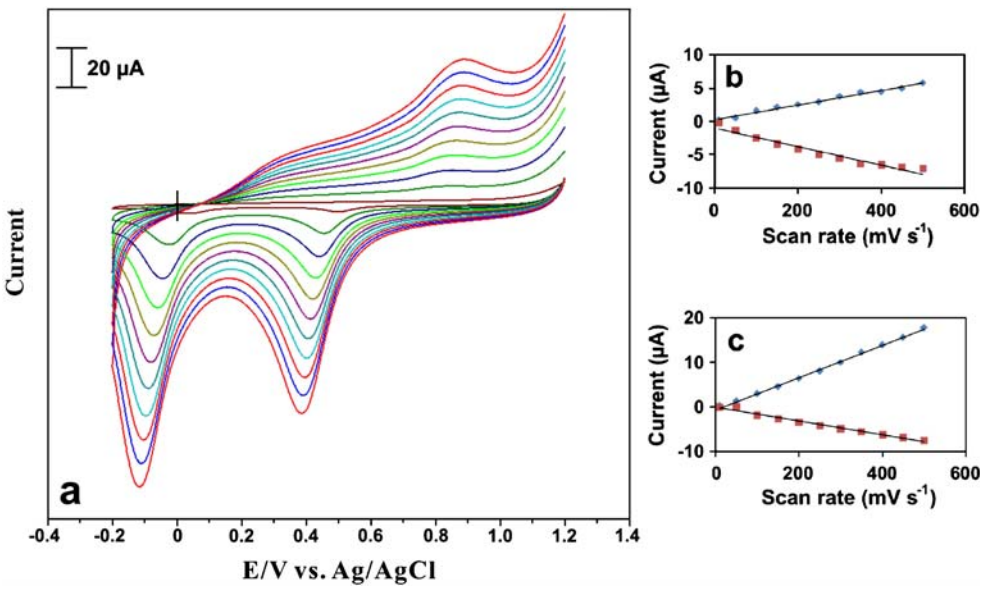

Fig. 2 **a** Cyclic voltammetric response of nanostructured Pt–Au hybrid film in pH 7.0 PBS at different scan rates: 10, 50, 100, 150, 200, 250, 300, 350, 400, 450, and 500 mV s^{-1}. Insets **b** and **c** show the plot of cathodic, anodic peak currents of platinum and gold vs scan rate

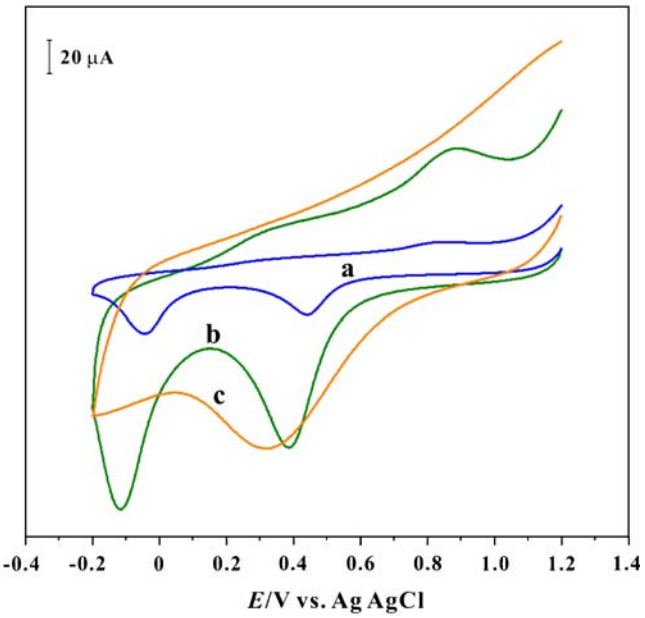

Fig. 3 CVs of the nanostructured Pt–Au hybrid film (presence of 2×10^{-4} mol l^{-1} L-cysteine) on GCE in pH 7 PBS at **a** 0.1 V s^{-1}, **b** 0.5 V s^{-1}, and **c** Pt–Au hybrid film in absence of L-cysteine at 0.5 V s^{-1}

nanostructured Pt–Au hybrid film was electrochemically active in pH 7.0 PBS solution. Here, the peak potentials of both platinum and gold were shifted to more negative side at higher scan rates. Figure 2b and c shows the plot of cathodic, anodic peak currents of platinum, gold vs scan rate, which show a close linear dependence with the scan rate. In addition, the linear behaviors of the plots indicate the reversible, diffusionless electron transfer process of platinum and gold with protons exchange, respectively. In addition, the voltammetric data were subjected to analysis by plotting log(i_p) vs log(v) the scan rate (data not shown) and the expected slope value obtained was close to 1, which exemplifies that it was a monolayer film. These results show that nanostructured Pt–Au hybrid film was electrochemically active in pH 7.0 PBS solutions.

To validate the importance of additive, the presence and absence of L-cysteine were examined during the Pt–Au film deposition process. In the absence of L-cysteine, it shows only a broad cathodic peak at 0.3 V (Fig. 3, curve c) (scan rate [0.5 V s^{-1}]), which was assumed to be the reduction peak of Au. At the same time, curves a and b show the Pt–Au hybrid film in presence of 2×10^{-4} mol l^{-1} L-cysteine in which we can see the reduction peaks of Pt and Au in clear manner. Thus, the presence of additive L-cysteine helps to bind the both particles on the electrode surface with good stability [29]. Further, the specific concentration of L-cysteine (2×10^{-4} mol l^{-1}) was resulted in the formation of cauliflower-shaped Pt nanoparticles. In addition, the higher concentration effects of L-cysteine were studied and the results are shown in Table 1. From Table 1, it was found that for the increasing concentrations of L-cysteine (>2×10^{-4} mol l^{-1}) fail to produce the bi-metallic nanoparticles. In particular, for the higher concentrations (4×10^{-4}, 6×10^{-4} mol $l^{-}1$) of L-cysteine, the solutions became turbid and immediate precipitations were occurred. From these results it was found that 2×10^{-4} mol l^{-1} of L-cysteine was suitable for the simultaneous deposition of both metallic nanoparticles, respectively.

Effect of solution pH and relationship between peak potentials

Figure 4(a) shows the CVs of nanostructured Pt–Au hybrid film in various pH solutions. Here, the values of E_{pa} and E_{pc} for Pt and Au nanoparticles were dependent on pH values of the buffer solution. In addition, the increase of the pH leads to a negative shift in potential for both the reduction and oxidation peaks of Pt and Au, respectively. Next, Fig. 4b and c shows the E_{pc}, E_{pa} of the platinum, gold plotted over a pH range of 1 to 13. Furthermore, the successive cycling (10 mV s^{-1}) applied on the Pt–Au hybrid film in pH 7.0 PBS and the CVs were recorded at the interval of 1 h. From those CVs, the values of I_{pa} and I_{pc} were noted and plotted against time (figure not shown). It was clear that for first 2 h the response of Pt–Au hybrid film was slightly decreasing and for the remaining hours it seemed to be stable. From these results, it was verified that the nanostructured Pt–Au hybrid film was electrochemically active and stable in pH 7.0 PBS. Also, pH 7.0 PBS is optimized pH solution for the proposed film.

Table 1 Concentration effects of L-cysteine during the Pt–Au hybrid film formation process

S. No	L-cysteine concentration in solution mixture (× 10^{-4} mol l^{-1})	Reduction peak potentials examined in pH 7.0 PBS (V)		Result
		Pt	Au	
1	2	−0.1	0.4	Presence of both Pt and Au nanoparticles
2	4	–	–	Solution became turbid and precipitation occurs
3	6	–	–	Solution became turbid and precipitation occurs

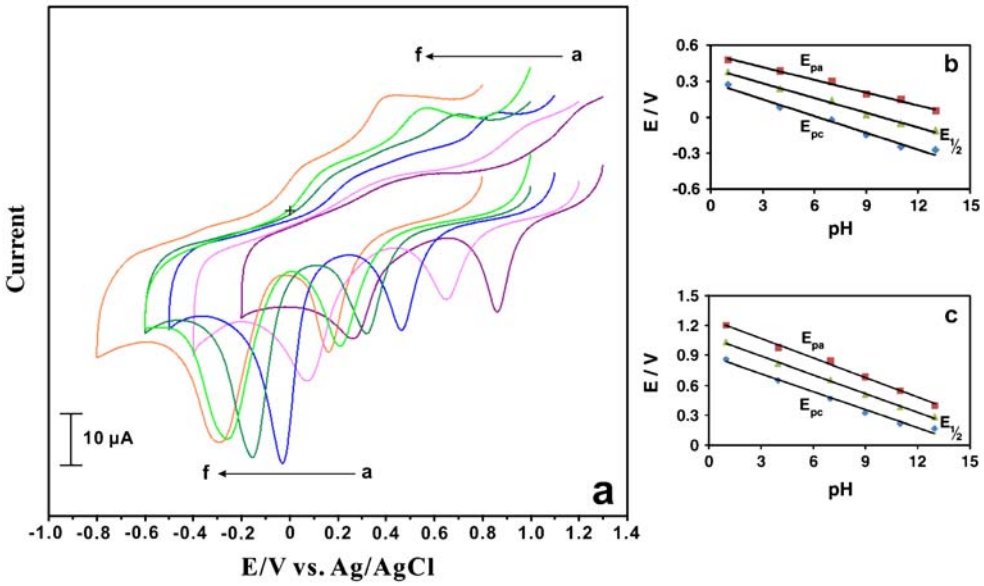

Fig. 4 **a** CVs of the nanostructured Pt–Au hybrid film on GCE in various pH buffer solutions (**a**–**f**) (pH 1, 4, 7, 9, 11, 13). The inset shows the plot of E_{pa}, E_{pc}, and $E_{1/2}$ vs pH for platinum (**b**) and gold (**c**)

SEM studies of nanostructured Pt–Au hybrid film

Figure 5a and b shows the typical SEM micrographs obtained for the nanostructured Pt–Au hybrid film electrodeposited on ITO. Here, Fig. 5a shows the 60-degree angle (magnification 20 K, 2 μm) and Fig. 5b shows the 90 degree angle (40 K, 2 μm) of the nanostructured Pt–Au hybrid film. The general inspection of these SEM results demonstrates that the increase of particle density concurrently with lowering the average particle size depends on the increasing concentration of additive L-cysteine. Here, the Pt nanoparticles were formed as cauliflower-shaped big and bright particles (250–400 nm). The flower-shaped structure of Pt nanoparticle formation was due to the higher concentrations of additive L-cysteine. In particular, the increase of L-cysteine concentration caused a significant enlargement of flower-shaped Pt nanoparticles. Furthermore, the small and low bright particles found in SEM images were Au nanoparticles (30–90 nm). Figure 5a and b SEM images clearly show the presence of flower-shaped Pt nanoparticles and the nano-Au particles. Finally, from these SEM results, the presence of flower-shaped Pt nano particles and nano Au was authenticated.

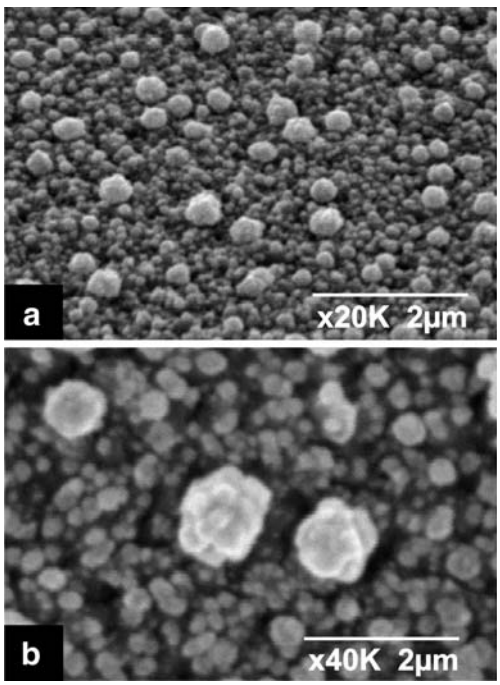

Fig. 5 **a** SEM images of nanostructured Pt–Au hybrid film (magnification 20 K, 60°). **b** Close view of flower-shaped nanoparticles in Pt–Au hybrid film (magnification 40 K, 90°)

EDS analysis

The energy-dispersive spectroscopy (EDS) was used to evaluate the chemical composition of nanostructured Pt–Au hybrid film. Figure 6 shows the EDS spectra of nanostructured Pt–Au hybrid film. Here, the EDS analysis confirms the percentage of deposition of both platinum and gold nanoparticles. Interpreting from the spectral data, the sharp and big peak designates the presence of gold and the small peak indicates the presence of Pt in the proposed film. From the EDS analysis, the approximate ratio of deposition of Pt and Au was 1:2. Finally, the EDS analysis result authenticates the presence of both Pt and Au [32].

Square wave voltammetric oxidation of EP and NEP

As the square wave voltammetry has more sensitivity and better resolution than cyclic voltammetry (CV), it was used

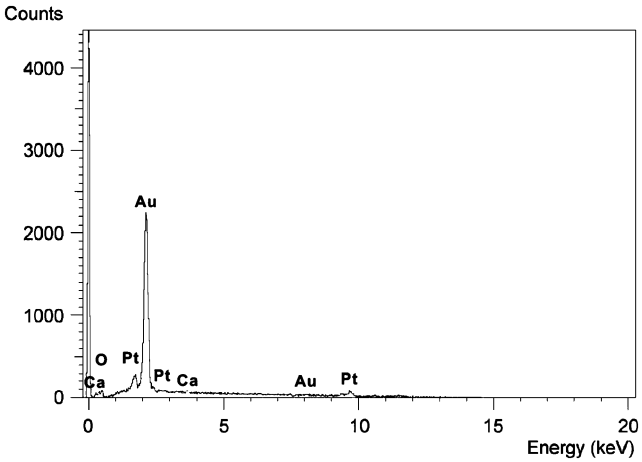

Fig. 6 EDS spectra of the nanostructured Pt–Au hybrid film on ITO

for the determination of EP and NEP on nanostructured Pt–Au hybrid film modified GCE. Figure 7a shows the square wave voltammograms (SWVs) of nanostructured Pt–Au hybrid film with various concentrations of EP. Here, the oxidation peak current increases with the increasing concentration of EP. Further, the oxidation peak currents of EP was measured and plotted against the concentration. As shown in Fig. 7c, the dependence of peak current vs concentration of EP was in the linear range of 0.39×10^{-4} to 2.6×10^{-4} mol l^{-1}, respectively. The linear regression equation was respectively expressed as I_{pa} (10^{-5} A) = 2.556 C (10^{-4} mol l^{-1}) + 0.662, with a correlation coefficient of R^2=0.998. Furthermore, the detection limit for EP (S/N=3) was found as 3.371×10^{-8} mol l^{-1}. In addition, the relative standard deviation (SD) for EP determination by using the Pt–Au hybrid film was found as 2.1%. Figure 7b shows the anodic peaks of NEP on nanostructured Pt–Au hybrid film. Here, the oxidation peak current increases linearly with the concentration range of 0.15×10^{-5} to 2.85×10^{-5} mol l^{-1}, respectively. Figure 7d shows the oxidation current vs concentration plot of NEP and the linear regression equations were expressed as I_{pa} (10^{-5} A) = 1.575C (10^{-5} mol l^{-1}) + 1.609, R^2=0.996. Here, the detection limit for NEP (S/N=3) is 1.267×10^{-8} mol l^{-1} and the relative SD for NEP for ten determination was 2.3%. From the SWV and detection limit result, it exemplifies that the nanostructured Pt–Au hybrid film was a remarkable film for the catalytic oxidation of EP and NEP.

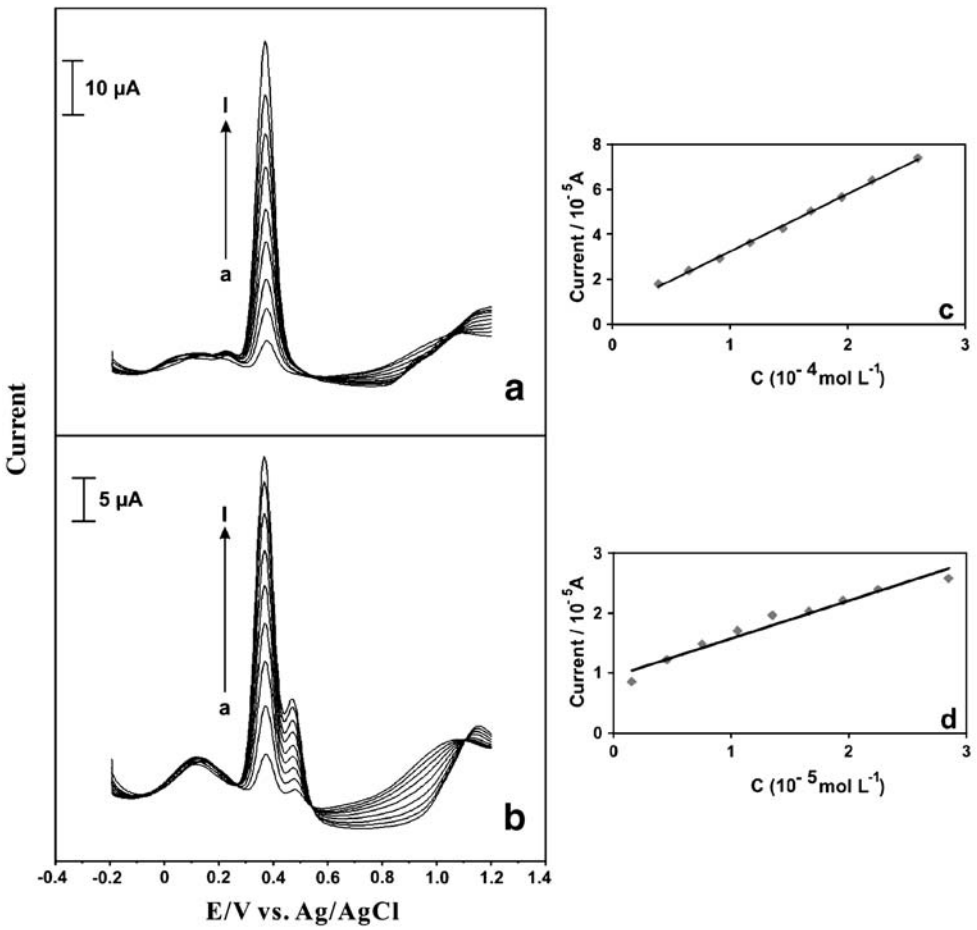

Fig. 7 **a** SWVs recorded for EP in the concentration range of (0.3, 0.65, 0.91, 1.17, 1.45, 1.69, 1.95, 2.21, and 2.6×10^{-4} mol l^{-1}) in pH 7.0 PBS solution, **c** calibration plot for EP, **b** SWVs of NEP in the concentration range of (0.15, 0.45, 0.75, 1.05, 1.35, 1.66, 1.95, 2.25 and 2.85×10^{-5} mol l^{-1}) in pH 7.0 PBS solution, and **d** calibration plot for NEP

Differential pulse voltammetric studies

The simultaneous determination of EP and NEP with AA is difficult at bare solid electrodes. But these compounds' peak potentials could be eminent at modified electrodes. According to the remarkable effects of pH on the peak potential, Pt–Au hybrid film show good separation of peak potentials in pH 7.0 PBS solutions. Thus, we have selected pH 7.0 PBS buffer solutions for the simultaneous determination of EP and NEP with AA. Here, the DPV technique could provide a better peak resolution and current sensitivity, which is most suitable for simultaneous determination of species in mixture. Figure 8a shows the DPV curves of AA and EP with concurrently changing the concentrations. Here, the peak separation between AA and EP was found to be about 137 mV, respectively. This separation was sufficient enough to allow the simultaneous determination of AA and EP in homogeneous solution. Further, the oxidation peak current increases linearly with the increasing concentrations of both AA and EP in the concentration range of 0.30×10^{-3} to 1.93×10^{-3} mol l^{-1}, 0.63×10^{-5} to 4×10^{-4} mol l^{-1}, respectively. Figure 8b and c shows the current vs concentration plot for both AA and EP, respectively. Further, the linear regression equation for AA and EP is expressed as I_{pa} (10^{-5} A) = 1.073C (10^{-5} mol l^{-1}) − 0.059, R^2=0.995 and as I_{pa} (10^{-5} A) = 0.569 C (10^{-4} mol l^{-1}) + 0.552, R^2=0.994, respectively. In addition, the detection limit (S/N=3) was found as 5.852×10^{-5} mol l^{-1} for AA and 9.762×10^{-7} mol l^{-1} for EP in AA–EP mixture. The comparison in the linear range and detection limit of

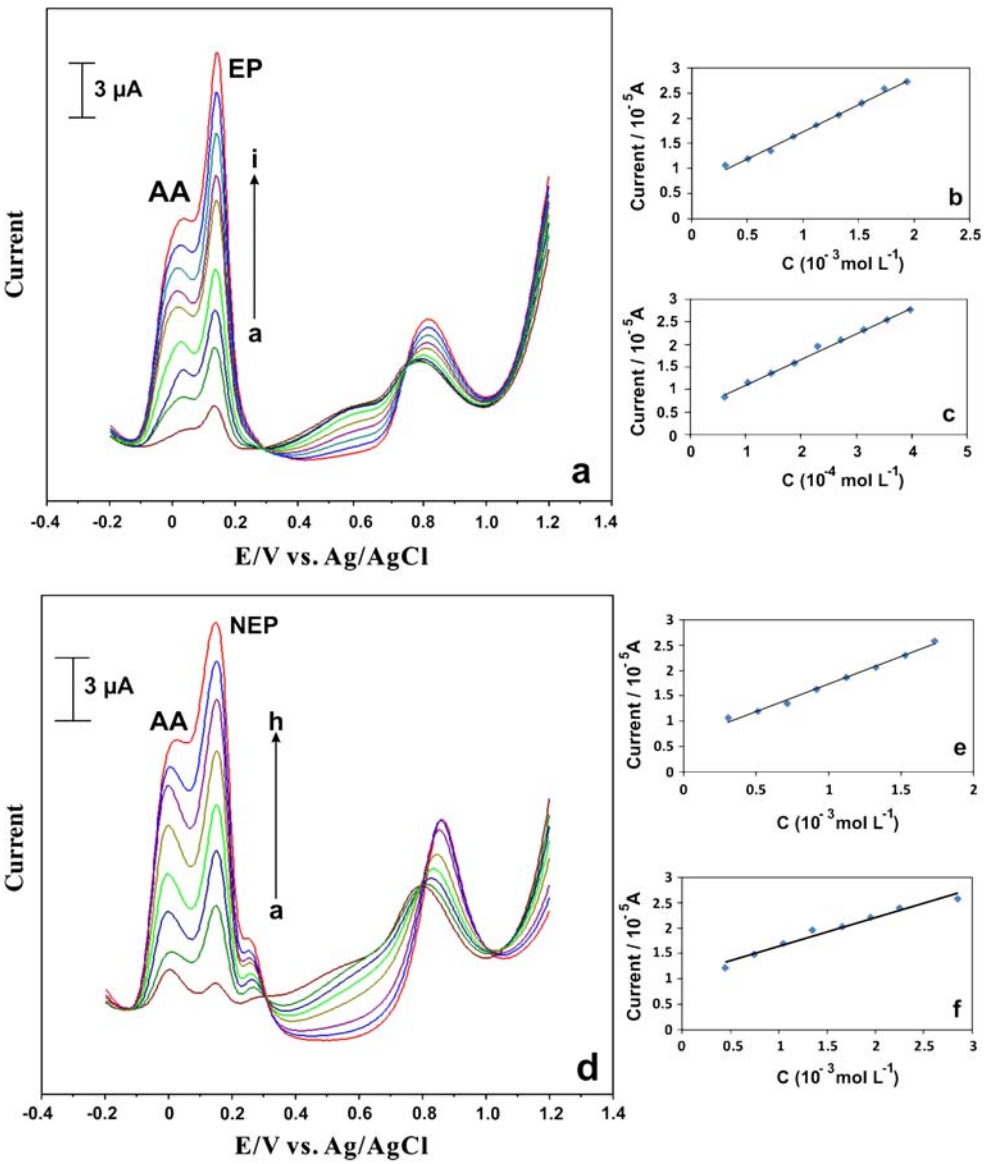

Fig. 8 **a** Anodic DPVs recorded for a mixture of AA (0.30, 0.51, 0.71, 0.91, 1.12, 1.32, 1.53, 1.73 and 1.93×10^{-3} mol l^{-1}) and EP (0.63, 1.05, 1.47, 1.89, 2.31, 2.73, 3.15, 3.57 and 4×10^{-4} mol l^{-1}) at Pt–Au hybrid film (pH 7.0 PBS), **b** and **c** show the calibration plot for AA and EP, **d** shows the DPVs recorded for a mixture of AA (0.30, 0.51, 0.71, 0.91, 1.12, 1.32, 1.53 and 1.73×10^{-3} mol l^{-1}) and NEP (0.45, 0.75, 1.05, 1.35, 1.66, 1.95, 2.25 and 2.85×10^{-4} mol l^{-1}) at Pt–Au hybrid film (pH 7.0 PBS), **e** and **f** show the calibration plot for AA and NEP

Table 2 Comparison table for simultaneous determination of AA and EP

Film	Linear range (mol l^{-1})		Detection limit (10^{-6} mol l^{-1})		Reference
	AA	EP	AA	EP	
Nano−Au/PPyox/GCE	–	$0.30–21\times10^{-6}$	–	0.030	[33]
Caffeic acid/GCE	$2.0\times10^{-5}–1.0\times10^{-3}$	$2.0\times10^{-6}–8.0\times10^{-5}$	7.0	0.2	[34]
Triazole/GE	$2.0\times10^{-5}–1.6\times10^{-4}$	$2.0\times10^{-5}–1.6\times10^{-4}$	–	–	[35]
DTDB/GCE	$1.0\times10^{-4}–1.0\times10^{-3}$	1.0×10^{-5}	–	–	[36]
MWCNT-PMB/GCE	$6\times10^{-4}–2.1\times10^{-3}$	$6\times10^{-4}–2.1\times10^{-3}$	27.9	46.4	[37]
Pt–Au hybrid film/GCE	$0.30–1.93\times10^{-3}$	$0.63–4\times10^{-4}$	58.52	0.97	This work

DTDB 5,5-ditetradecyl-2-(2-trimethyl-ammonioethyl)-1,3-dioxane bromide, *PMB* polymethylene blue, *MWCNT* multi-walled carbon nanotube, *PPYox* polypyrrole

AA and EP detections at modified electrodes is listed in Table 2. As seen in this comparison table, this type of Pt–Au hybrid film modified GCE showed good linear range of detection with average detection limits for both EP and NEP determinations in presence of AA.

Next attempt was taken to detect AA and NEP. Figure 8d shows the DPV curves for the simultaneous determination of AA and NEP in pH 7.0 PBS buffer solution. Here the oxidation peak current increases linearly with the increasing concentration of AA and NEP in the range of 0.3×10^{-3} to 1.73×10^{-3} mol l^{-1}, 0.45×10^{-5} to 2.85×10^{-4} mol l^{-1}, respectively. Peak to peak separation between the oxidation peak potentials of AA–NEP was found as 150 mV. Further the Fig. 8(e) and (f) shows the calibration curves for both AA and NEP. The linear regression equations were found as I_{pa} (10^{-5} A) =1.080 C (10^{-4} mol l^{-1}) − 0.065, R^2=0.994 for (AA); I_{pa} (10^{-5} A) =0.567 C (10^{-4} mol l^{-1}) + 1.608, R^2= 0.97 for NEP. Furthermore, the detection limit (S/N=3) was found as 9.07×10^{-6} mol l^{-1} for AA and 5.38×10^{-8} mol l^{-1} for NEP in AA–NEP mixture. From these DPV results, it was ascertained that the nanostructured Pt–Au hybrid film succeeded in separating the AA–EP and AA–NEP successfully without any fouling effect. To validate the reproducibility results, three GC electrodes were electrochemically deposited with Pt–Au hybrid film and their responses toward the oxidation of EP and NEP with AA were investigated. The peak to peak separation between the voltammetric signals of EP, NEP with AA remained almost the same for all the three electrodes, which authenticates that the results were reproducible.

Real-sample analysis

To evaluate the practical analytical performance of Pt–Au hybrid film, the real-sample analysis was done for the determination of EP in practical samples such as EP injection solution and vitamin C tablets. The real-sample analysis data for EP injection solution (1 mg ml^{-1}) in the presence of vitamin C solution (4.0×10^{-4} mol l^{-1}) results are listed in Table 3. From these results, it is revealed that the nanostructured Pt–Au hybrid film shows significant catalytic activity for real-sample analysis, and the recoveries were found satisfactory.

Conclusions

In conclusion, this study has demonstrated the fabrication of nanostructured Pt–Au hybrid film sensor on GCE and ITO electrode surface based on the concentration effects of additive L-cysteine, which was resulted in the formation of cauliflower-shaped Pt particles. Also, the proposed film-modified GCE exhibited good electrocatalytic activity in pH 7.0 PBS and showed efficient electrocatalysis for epinephrine, norepinephrine detection, and individual and simultaneous determination of both catecholamines in the presence of ascorbic acid. The calibration plots of current vs concentrations for EP and NEP with AA showed that Pt–Au hybrid film could be effectively applied for the simultaneous determination process. In addition, the proposed film exhibits satisfactory detection limits for the

Table 3 Determination of EP in epinephrine injection (in presence of 4.0×10^{-4} mol l^{-1} vitamin C solution)

S. No	Added (× 10^{-5} mol l^{-1})	Found (× 10^{-5} mol l^{-1})	Recovery (%)
1	1.30	1.29	99.23
2	2.30	2.40	104.34
3	4.20	4.00	95.23
4	6.00	6.10	101.66

simultaneous determination of EP and NEP in the presence of large amounts of AA. Finally, this work illustrates a simple and novel approach for the catecholamine sensor development based on nanostructured Pt–Au hybrid film.

Acknowledgments This work was supported by National Science Council of Taiwan (ROC).

References

1. Bergquist J, Sciubisz A, Kaczor A, Silberring J (2002) J Neurosci Methods 15:1
2. Solich P, Polydorou CH, Koupparis MA (2000) J Pharm Biomed Anal 22:781
3. Yang J, Zhang G, Wu X, Huang F, Lin C, Cao X, Sun L, Ding Y (1998) Anal Chim Acta 363:105
4. Sabbioni C, Saracino MA, Mandrioli R, Pinzauti S, Furlanetto S, Gerra G, Raggi MA (2004) J Chromatogr A 1032:65
5. Lin CE, Fang IJ, Deng YJ, Liao WS, Cheng HT, Huang WP (2004) J Chromatogr A 1051:85
6. Michalowski J, Halaburda P (2001) Talanta 55:1165
7. Li F, Cui H, Lin XQ (2002) Anal Chim Acta 471:187
8. Ni JA, Ju HX, Chen HY, Leech D (1999) Anal Chim Acta 378:151
9. Mateo JVG, Kojlo A (1997) J Pharm Biomed Anal 15:1821
10. Mo Z, Long X, Zhang M (1999) Talanta 48:643
11. Tsai YC, Chiu CC (2007) Sens Actuators B Chem 125:10
12. Zhu M, Huang X, Li J, Shen H (1997) Anal Chim Acta 357:261
13. Ye BX, Xia P, Lin L (2000) Microchem J 64:125
14. Zhang S, Xu Q, Zhang W, Jin L, Jin J-Y (2001) Anal Chim Acta 427:45
15. Wang H, Jin H, Zhang HS (1999) J Anal Chem 365:682
16. Guan CL, Quyang J, Li QL, Liu BH, Baeyens WR (2000) Talanta 50:1197
17. Arya SP, Mahajan M, Jain P (2001) Anal Chim Acta 427:245
18. Fontannaz P, Kilinc T, Heudi O (2006) Food Chem 94:626
19. Lopes P, Drinkine J, Saucier C, Glories Y (2006) Anal Chim Acta 555:242
20. Zhang HM, Zhou XL, Hui RT, Li NQ, Liu DP (2002) Talanta 56:1081
21. Kawage TK, Wightman RM (1994) Talanta 41:865
22. Luo H, Shi Z, Ni N, Gu Z, Zhuang Q (2001) Anal Chem 73:915
23. Wang J, Li M, Shi Z, Li N, Gu Z (2002) Electroanalysis 14:225
24. Valentini F, Amine A, Orlanducci S, Terranova ML, Palleschi G (2003) Anal Chem 75:5413
25. Raoof JB, Ojani R, Nadimi SR (2005) Electrochim Acta 50:4694
26. Lu LP, Wang SQ, Lin XQ (2004) Anal Chim Acta 519:161
27. Oyama M (2007) Rev Polarogr 53:1
28. El-Deab MS, Sotomura T, Ohsaka T (2005) J Electrochem Soc 152:C1
29. Thiagarajan S, Chen SM (2007) Talanta 74:222
30. Luo J, Njoki PN, Mott D, Wang L, Zhong CJ (2006) Langmuir 22:2892
31. Luo J, Njoki PN, Mott D, Wang L Zhong CJ (2006) Electrochem Commun 8:581
32. Chikae M, Idegami K, Kerman K, Nagatani N, Ishikawa M, Takamura Y, Tamiya E (2006) Electrochem Commun 8:1375
33. Li J, Lin XQ (2007) Anal Chim Acta 596:222
34. Ren W, Luo HQ, Li NB (2006) Biosens Bioelectron 21:1086
35. Sun YX, Wang SF, Zhang XH, Huang YF (2006) Sens Actuators B 113:156
36. Gong J, Lin X (2004) Electrochim Acta 49:4351
37. Yogeswaran U, Chen SM (2008) Sens Actuators B Chem 130:739